

Electromagnetic Modeling of Rat's Head: Comparison of Formulations and Models

David KURATKO¹, Daniel Krzysztof WOJCIK^{1,2}, Jaroslav LACIK¹, Vlastimil KOUDELKA³

¹ Dept. of Radio Electronics, Brno University of Technology, Technická 12, 616 00 Brno, Czech Republic

² Nencki Institute of Experimental Biology of Polish Academy of Sciences, Warsaw, Poland

³ National Institute of Mental Health, Topolová 748, 250 67 Klecany, Czech Republic

xkurat01@stud.feec.vutbr.cz

Submitted December 14, 2018 / Accepted July 25, 2019

Abstract. *Reliable inverse imaging of source currents in rat's brain requires sufficiently accurate and CPU-time moderate forward models of fields to calibrate inverse solvers. In this paper, we compare different mathematical formulations of the electromagnetic problem related to the analysis of brain waves (static, quasi-static, full-wave) and various meshes differing in the density, the type and the geometrical accuracy.*

A sufficiently accurate model of brain waves is then completed by the cerebrospinal fluid and the skull. The resultant composite model of rat's head with properly set electrical parameters has to be calibrated by the outputs of measurements. That way, a realistic electromagnetic model of the head of a live rat can be obtained.

Keywords

Forward brain model, rat's head, numerical analysis, Maxwell equations

1. Introduction

In the open literature, methods for solving both the forward problem and the inverse one in electroencephalography (EEG) are described for human beings in detail. Current densities excited by equivalent source dipoles are expressed by Poisson's equation with full-tensor anisotropic conductivity. The human skull is approximated by a three-shell concentric spherical model (the skin, the skull, and the brain). For layered spherical anisotropic volume conductors, semi-analytical and numerical solutions are available.

However, neither forward models nor inverse solvers have been properly calibrated and tested in human beings since in-vivo experiments exploiting deep electrodes are not allowed. Thus, all electromagnetic quantities in human beings have been measured indirectly.

In order to implement direct measurements, experiments can be carried out on rats. Nevertheless, there are

significant differences between the brain of a human and a brain of a rat:

- Shape and size of brains differ significantly. Due to shape and size limitations, animal brains can be accessed from the top of the skull only.
- Location of source currents in brains is considered differently. In the EEG studies of the human brain, currents are assumed to flow in the cortex mainly. Subcortical sources are ignored because of limited sensitivity of EEG to the signals they generate. In case of the animal brain, the whole volume of the brain can be investigated.
- Electromagnetic parameters of live brain tissues have not been determined with a sufficient accuracy yet. Therefore, numerical models and phantoms have to be calibrated.
- The animal head is covered by muscles. Since muscles distort EEG signals, measurements have to be performed on a shaved skin or on the brain surface directly.

The above-given reasons are the main motivation for the research of brain waves propagating in the head of a rat.

Brain waves can be measured on rat's head surface in form of electrical potentials [1]. Localization of brain wave sources requires a forward model and an inverse solver [2]. The forward model is aimed to calculate the potentials at the surface electrodes from known source parameters.

In the matrix form, the forward model can be expressed as [3]

$$\mathbf{B} = \mathbf{L} \cdot \mathbf{J} \quad (1)$$

where \mathbf{B} is the matrix of simultaneously acquired time series of potentials measured in independent channels, \mathbf{J} is the current matrix and \mathbf{L} is the so-called lead-field matrix.

The lead-field matrix is essential for solving the inverse problem

$$\mathbf{J} = \mathbf{L}^{-1} \cdot \mathbf{B}. \quad (2)$$

The solution is asked to determine wave sources \mathbf{J} in the brain from electrical potentials measured on the surface \mathbf{B} .

The lead-field matrix can be evaluated by several simulations of the forward model with varying positions of excitation sources. The paper is focused on the forward model.

At present, most models of brain waves are based on the quasi-static formulation. Thus, the relationship between the brain current sources and corresponding potentials on the brain surface is given by Poisson's equation:

- In the review paper [4], basic principles of forward modeling are given. Attention is turned to the generation of EEG, Poisson's equation, a three-shell spherical head model and proper application of numerical methods (BEM, FEM, FDM), especially
- In [5], the conductivity profile in the somatosensory barrel cortex of the Wistar rat is evaluated. First, boundaries of a six-layer barrel cortex are determined as spherical ones using fluorescent Nissl staining images. After injecting the current and recording corresponding potentials by electrodes, the analytical formula in a non-linear optimization method is used to estimate the conductivity profile in a spherical model (radii identified with fluorescent Nissl staining images).

In [5], the influence of the estimated conductivity profile to the current source density (CSD) is also demonstrated when forward modeling is included.

- In [6], the extensive description of measuring techniques of the neural activity is provided. The most important part relates to the EEG and MEG forward modeling. Additionally, the intracellular and extracellular recording, CSD and the most popular techniques used to measure neuronal activity (functional magnetic resonance imaging, calcium imaging, etc.) are reviewed.

In majority of today's models, potentials are calculated by the boundary element method (BEM) on the surface only. Hence, no anisotropy of brain tissues can be considered. Moreover, the models cannot include potentials inside the head when stimulating electrodes are used, for example. Therefore the finite integration technique (FIT) was used for simulations presented in the paper.

For a human head, an analytical approximate model consisting of three concentric spheres is known [4]. Since the head of the rat cannot be approximated by a sphere sufficiently [7–10], more realistic approximations have to be used. Such approximations have not been described in the open literature sufficiently yet.

Furthermore, a recent paper [11] on the time-domain full-wave formulation of brain waves showed significantly different results compared to quasi-static approximations of a sphere and a slab.

Due to these reasons, we decided to compare:

- Outputs of all solvers of Maxwell equations available in the CST Studio Suite [12] with an analytical solution of electric field intensity excited by a dipole inside a spherical model of a head. The comparison of results should answer the question what solver should be selected to obtain reliable results with minimum CPU costs.
- Simulations of rat's brain model of a realistic shape [7–10] and a spherical one. The comparison should show dependencies that cannot be clearly provided by a spherical model (sphere is an insufficient approximation of the shape of rat's brain).
- Rat's brain models of a different geometrical accuracy and a mesh density. The comparison of results should answer the question what geometrical accuracy of the model is needed to calibrate the imaging procedure.
- The isolated brain and the complete head. The brain model was embedded into the cerebrospinal fluid and the skull. The fluid and the skull differ in the electrical conductivity and the relative permittivity. The comparison of results should answer the question what way the fluid and the skull transform the electric field intensity measured on the brain surface.

Preliminary results of the above-specified research were discussed in [2], and outputs of discussions were reflected in the paper.

2. Formulation of Maxwell Equations, 3D Models and Simulation Setup

2.1 Formulation of Maxwell Equations

The brain can be understood as a volumetric source of a current produced by populations of neurons. Various frequencies of electromagnetic waves can be observed due to the complex behavior of the brain. Generally, many studies on neural oscillations conclude that deeper parts of the brain excite electromagnetic waves with rather lower frequencies and the frequency rises in the evolutionary younger areas closer to the brain surface [13]. However, appropriate mapping of frequencies is not available due to the complexity and inter-individual variability of the brain.

Brain waves propagate at frequencies from 0.1 Hz to 100 Hz. However, the power of the electroencephalograph (EEG) signal decreases with the increasing frequency by the factor of $1/f$ [14]. Thus, rat's brain was decided to be simulated at the frequency 10 Hz which corresponds to the known peak in the spectral power of a human EEG.

Figure 1 shows an overview of formulations which can be used for the development of electromagnetic models

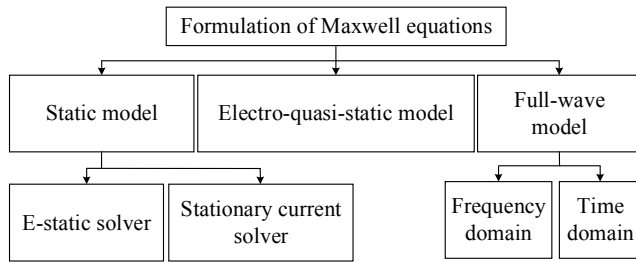


Fig. 1. Overview of formulations used for the development of electromagnetic models of rat’s brain (CST terminology).

of rat’s brain in the CST Studio Suite [12]. The models resulting from these formulations differ in the accuracy and CPU-time demands. The models can be characterized as follows:

- The static model represents the highest simplification of Maxwell equations. The static model is related to two solvers of the CST Studio Suite [12], to the electrostatics field solver (field excited by stationary charges) and the stationary current solver (field excited by direct currents). Brain waves can be characterized by the spatial distribution of the electric potential or the electric field intensity.
- The electro-quasi-static model neglects displacement currents, and brain waves are represented by the spatial distribution of the field intensity.
- Full-wave models can be formulated in the frequency domain (a steady state at a single harmonic frequency) and the time domain (a transient state with an arbitrary time response). In both the domains, brain waves can be displayed in form of time-varying spatial distributions of field intensities.

In order to develop the full-wave time-domain model, the frequency scaling method [11] was applied since the low-frequency breakdown can occur, and the solution of Maxwell equations can diverge.

The frequency scaling method [11] is based on scaling the relative permittivity ϵ_{rsc} of the brain tissue ϵ_r

$$\epsilon_{rsc} = \epsilon_r \frac{f}{f_{sc}} \tag{3}$$

Here, f denotes the original frequency (i.e., the frequency of brain waves) and f_{sc} corresponds to the frequency of simulation. Thanks to this scaling, the simulation can be shifted from Hz to MHz. If brain waves are simulated at higher frequencies, then the low-frequency breakdown is overcome, and the simulation is accelerated.

After the simulation, the resulting quantities have to be recalculated according to the following equation [11]:

$$X = X_{sc} \frac{f}{f_{sc}} \tag{4}$$

Here, X represents the observed quantity (intensity of

electric or magnetic field) at the original frequency f , and X_{sc} corresponds to the quantity of the simulation at f_{sc} .

2.2 3D Models

The brain models are based on the magnetic resonance images (MRI) processed with Blender [15], MeshLab [16], Autodesk MeshMixer [17] and Autodesk Fusion 360 [18].

After removing duplicated surfaces and edges of elements, correcting unevenness, protrusions, sharp edges and modifying the orientation of mesh elements, a new mesh can be generated to preserve anatomy of rat’s brain. Brain models were resized to the length $l = 27$ mm, the width $w = 15$ mm and the height $h = 10$ mm which correspond to approximate dimensions of the brain of an adult rat.

Two brain models differing in the mesh density were generated (see Fig. 2). The bold curve in the center of models represents the trajectory followed when electric field intensity E on the brain surface is measured. The coordinate p_1 runs from left to right.

To compare the model of the isolated brain and the complete head, the brain model #1 was embedded into the cerebrospinal fluid and the skull. Since the brain model #1 and the skull model come from different MRI scans of rat’s head, the brain was proportionally scaled to fit the cavity in the skull. The free space between the brain and the skull was filled in by the cerebrospinal fluid. After that, the brain model #1, the cerebrospinal fluid and the skull were converted to voxels. Thanks to the conversion, the brain, the fluid and the skull can be aligned (potential gaps can be eliminated), and simulations are accelerated.

In Fig. 3, the composite model of the complete head is shown. The model consists of the brain, the fluid and the skull converted into voxels with the length of the edge

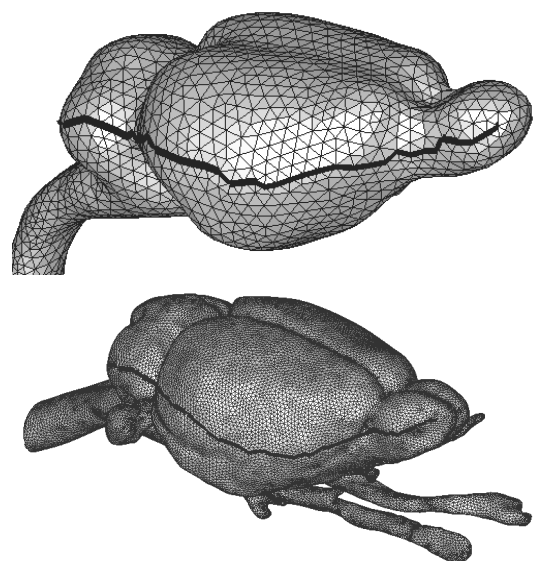


Fig. 2. Models of rat’s brain. Top: simplified rough model (#1). Bottom: detailed fine model (#2).

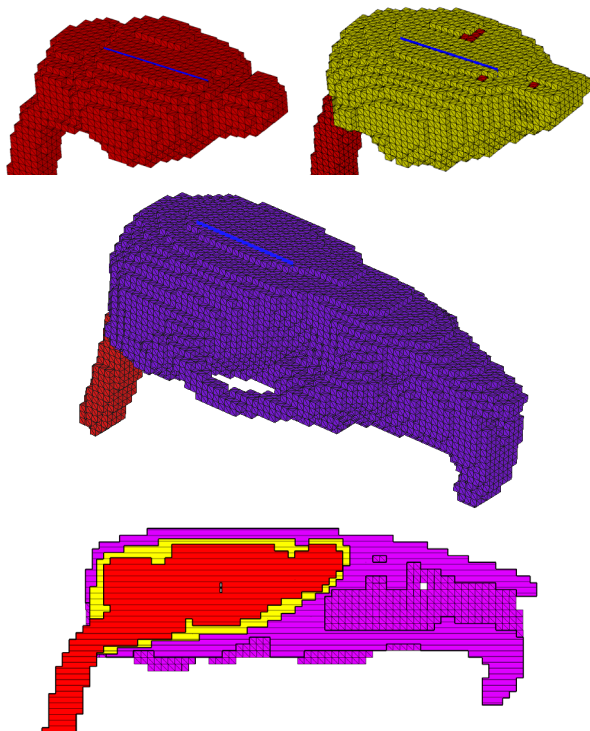


Fig. 3. Voxel models. Top: the brain (left), the cerebrospinal fluid (right). Center: the skull. Bottom: vertical cut of the composite model crossing the center of the head.

$l_e = 0.7$ mm. The bottom picture in Fig. 3 proves that all the models are properly aligned thanks to the conversion to voxels.

In order to validate simulation results, a simplified spherical model of rat's brain was created. The model consisted of a homogeneous sphere with radius $r = 50$ mm placed at the origin of coordinates.

2.3 Simulation Setup

The group of active neurons can be modelled as a current dipole [4], [6], [19] which excites an electrical field propagating to the surface of rat's brain. The dipole has the total length $l = 1$ mm with the gap $g = 0.1$ mm between arms and the diameter of arms $d = 0.1$ mm.

In simulations with the sphere, the horizontal dipole in origin of coordinates played the role of a source. In all other simulations, fields were excited by the vertical dipole in the center of the brain. Sources excited the dipole moment $m = 1$ A·m. Outputs of all solvers were converted to the distribution of electric field intensity.

Electrical parameters of rat's tissues were approximated by the corresponding parameters of human tissues [4], [20], [21]:

- All tissues and formulations considered the relative permeability $\mu_r = 1$.
- The electric conductivity was $\sigma = 0.33$ S/m for the brain and the sphere, $\sigma = 1.79$ S/m for the cerebrospinal fluid, and $\sigma = 0.0174$ S/m for the skull.

Model	Formulation	
	Static, quasi-static & frequency domain	Time domain
Sphere	1	$1 \cdot 10^{-6}$
Brain	$4.07 \cdot 10^7$	$4.07 \cdot 10^2$
Cerebrospinal fluid	$1.09 \cdot 10^2$	–
Skull	$5.51 \cdot 10^4$	–

Tab. 1. Relative permittivity ϵ_r of models for all investigated formulations [22].

- The relative permittivity was $\epsilon_r = 1$ for the sphere, $\epsilon_r = 4.07 \cdot 10^7$ for the brain, $\epsilon_r = 1.09 \cdot 10^2$ for the cerebrospinal fluid, and $\epsilon_r = 5.51 \cdot 10^4$ for the skull.

The frequency tends to zero in the static formulation. Since relative permittivity is unknown at zero frequency, the values corresponding to 10 Hz were used.

Applying the frequency scaling (3) in the full-wave time-domain formulation, the simulation was transferred from 10 Hz to 10 MHz and the relative permittivity was shifted by six orders.

Due to the complexity and inter-individual variability of the brain, general value of the relative permittivity can be hardly determined. From the electrical viewpoint, the gray matter is the most significant part since neural activities are formed there [4]. In the simulations with the model #1, the model #2 and the complete model, the relative permittivity of the gray matter was therefore used.

3. Simulation Results

3.1 Spherical Model

In Fig. 4, the analytical solution of electric field intensity inside the sphere is compared with outputs of solvers available in CST Studio Suite [12].

The electric field intensity E was measured in plane of the dipole along x axis. The results indicate the minimum

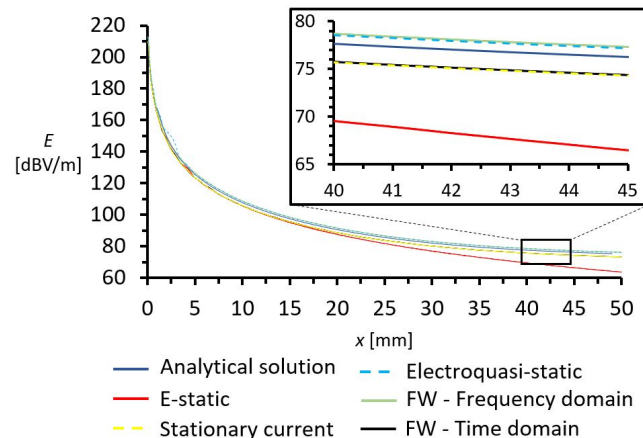


Fig. 4. Dependency of electric field intensity on the distance from source for spherical model. Analytical solution versus solvers available in CST Studio Suite.

Solver	CPU time [mm:ss]	Percentage deviation from analytic solution
E-static	01:21	6.1
Stationary current	02:05	2.2
Electro-quasi-static	01:17	1.2
Full-wave, frequency domain	30:45	1.2
Full-wave, time domain	03:44	2.1

Tab. 2. Comparison of CPU-time demands and relative errors of solvers available in the CST Studio Suite.

difference between the electro-quasi-static solver and the analytical solution. On the other hand, the maximum difference appears in case of the static model.

Table 2 compares CPU-time demands and percentage deviations from the analytical solution for all solvers available in the CST Studio Suite. The comparison shows that outputs of the full-wave frequency-domain solver and the electro-quasi-static solver differ from the analytical results similarly, but CPU-time demands of the electro-quasi-static solver are 30× lower approximately.

The full-wave time-domain solver shows a higher error than the frequency-domain one due to the application of frequency scaling. The relative error of the full-wave time-domain solver corresponds to the error of the stationary current solver.

3.2 Isolated Brain

Figure 5 shows the influence of the number of tetrahedrons used for meshing. For this comparison, the electro-quasi-static solver and the brain model #1 were used. The mesh density is specified by the number of cells per the maximum edge of the model box. The meshing procedure is based on the surface model which is identical for all simulations.

The comparison shows that the model with 94 084 tetrahedrons provides results similar to meshes with highest numbers of elements. Therefore, the mesh consisting of 94 084 elements can be considered as sufficiently dense.

Table 3 summarizes influence of the number of mesh elements on the accuracy and CPU-time demands of simulations. The simulation with the highest number of tetrahedrons is used as a reference for relative error calculation. The results show that the model with the highest number of tetrahedrons needs the highest CPU time. Since the relative error of the model with 94 084 elements is acceptable, this number of tetrahedrons can be considered to be sufficient for forward modeling.

Figure 6 compares simulations by the electro-quasi-static solver for models #1 and #2. The discrepancy at $p_1 = 6$ mm and $p_1 = 26$ mm is caused by transitions from olfactory bulbs to the central part of the brain, and from the central part of the brain to cerebellum, respectively (see Fig. 2). These transitions are represented by grooves in 3D

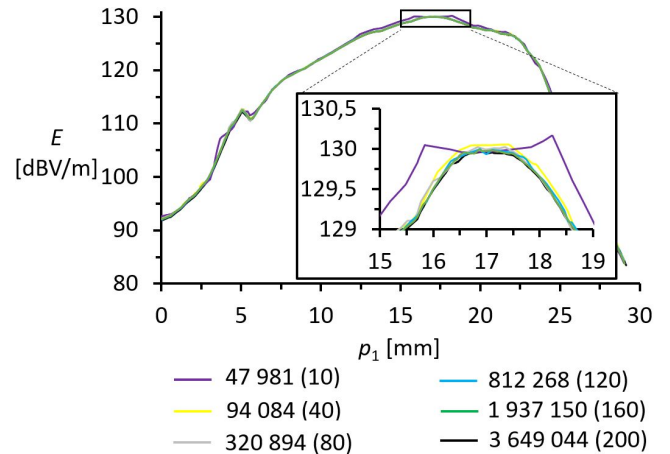


Fig. 5. Electric field intensity along the measuring trajectory p_1 for the simplified rough model #1: influence of the number of tetrahedrons.

Mesh elements for model #1 [-]	CPU time [mm:ss]	Cells per max. edge [-]	Relative error [%]
47 981	00:10	10	0.40
94 084	00:20	40	0.17
320 894	00:54	80	0.12
812 268	02:48	120	0.09
1 937 150	07:09	160	0.11
3 649 044	16:01	200	-

Tab. 3. Influence of the number of mesh elements on the accuracy and CPU-time demands of simulations.

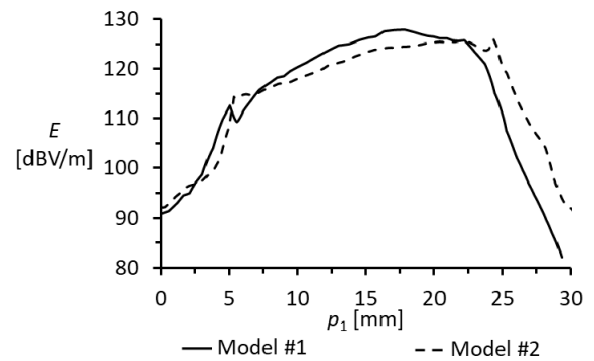


Fig. 6. Electric field intensity along the measuring trajectory p_1 for model #1 (solid) and model #2 (dashed) when electro-quasi-static solver is used.

models. The surface of the brain is closer to the dipole, and the electric field intensity is higher there. Since the discrepancy is small compared to the size of grooves, the rough brain model can be considered to be sufficient for forward modeling.

Since rat's brain cannot be approximated by a sphere as the human brain, more realistic models of rat's brain have to be used. Figure 7 shows electric field intensity along the trajectory p_1 computed by all the solvers for the simplified rough model (#1) in the top chart, and for the refined model (#2) in the bottom chart. The measuring trajectory p_1 corresponds to the bold curve on the surface

of brain models in Fig. 2 and is measured from left to right. Comparison of both the dependencies shows the following:

- The e-static solver and the stationary current one give comparable results both for the rough model #1 and the fine model #2. Simulation of the spherical model shows a lower relative error in case of the stationary current solver than the e-static one.
- The electro-quasi-static solver and the full-wave frequency domain one give comparable results for both the models.
- Accuracy of the full-wave time domain solver is influenced by the model geometry. For the fine model #2, the accuracy corresponds to the e-static solver and the stationary current one along the entire length of the measuring trajectory p_1 . For the rough model #1, the accuracy is closer to the electro-quasi-static solver in the middle of the measuring trajectory $p_1 \in (6 - 25)$ mm. In the rest of the measuring trajectory p_1 , the accuracy corresponds to the e-static solver.

Error of the full-wave time-domain solver is caused by the frequency scaling [11] from 10 Hz to 10 MHz. At this frequency, the wavelength is much smaller and the interaction with the model is stronger.

Since both the model #1 and the model #2 is homogeneous and isotropic, higher values of electric field intensity E correspond to active areas in a shorter distance. Therefore, the highest values of electric field intensity E can be measured in the central part of the measuring trajectory p_1 which is in the shortest distance from the dipole located in the center of the brain. Obviously, simulations with realistic 3D models of rat's brain cannot correspond to simulations with the spherical model.

The electro-quasi-static solver [12] can reach the best accuracy within the lowest CPU time, but does not allow to include lumped elements into simulation which is useful when expanding the forward model (EEG measurement elements, RLC circuits simulating coupling between cables, etc.). Fortunately, inclusion of lumped elements is supported by the full-wave frequency-domain solver which reaches a comparable relative error, and can be an alternative when the CPU time is not the priority.

An overview of CPU-time demands and relative errors of different solvers is listed in Tab. 4. The error is related to outputs of the electro-quasi-static solver.

The electro-quasi static solver requires a similar CPU time compared to the full-wave frequency-domain solver when the fine model #2 is simulated. In case of the rough model #1, CPU-time requirements of the electro-quasi static solver are significantly lower. Thus, the full-wave frequency-domain solver is CPU-time effective when complexity of a 3D model is higher (e.g., when a skull, a cerebrospinal fluid, measuring electrodes, anisotropic properties are added).

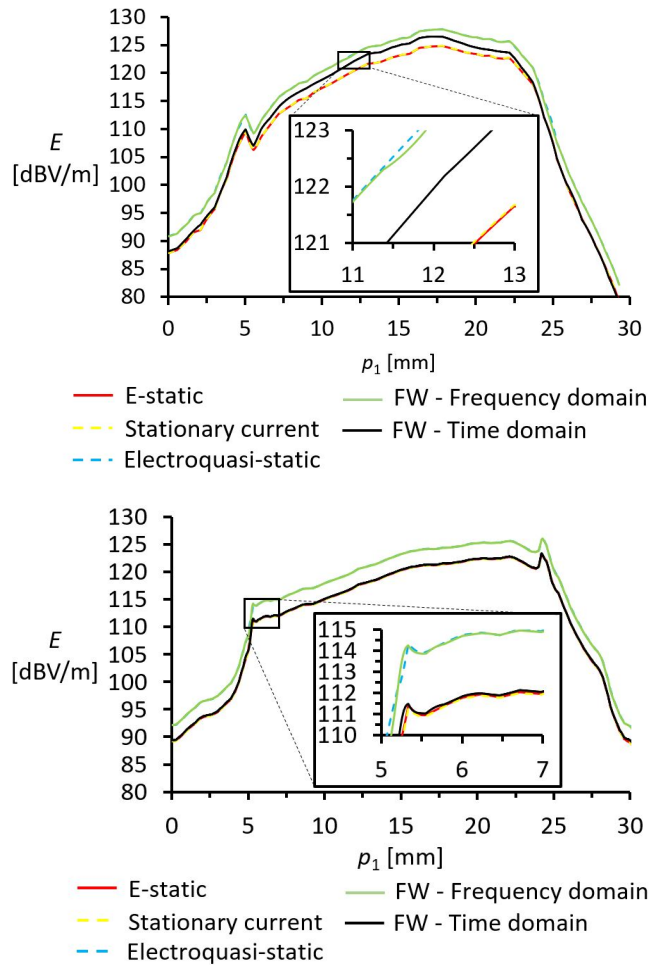


Fig. 7. Electric field intensity along the measuring trajectory p_1 . Top: the simplified rough model (#1). Bottom: the detailed fine model (#2).

Solver	Model #1		Model #2	
	CPU time [hh:mm:ss]	Percent. error	CPU time [hh:mm:ss]	Percent. error
E-static	00:00:14	2.7	00:09:11	2.6
Stationary current	00:00:11	2.6	00:09:06	2.7
Electro-quasi-static	00:00:20	–	00:10:46	–
Full-wave frequency-domain	00:05:43	0.1	00:13:23	0.1
Full-wave time-domain	00:01:10	1.8	01:46:22	2.5

Tab. 4. Comparison of CPU-time demands and the relative errors of different solvers for both models.

The full-wave time-domain solver shows much higher CPU-time demands for the fine model #2 in comparison with the rough model #1. Considering both the accuracy and CPU time demands, the full-wave time-domain solver seems to be inappropriate for complex forward modeling.

Figures 8 and 9 show the distribution of computed electric field intensity both for the model #1 and the model #2. On the top, electric field distribution on the surface of the brain is depicted. Other figures visualize field distribution in the coronal cut, the axial cut and the sagittal cut passing the center of the brain.

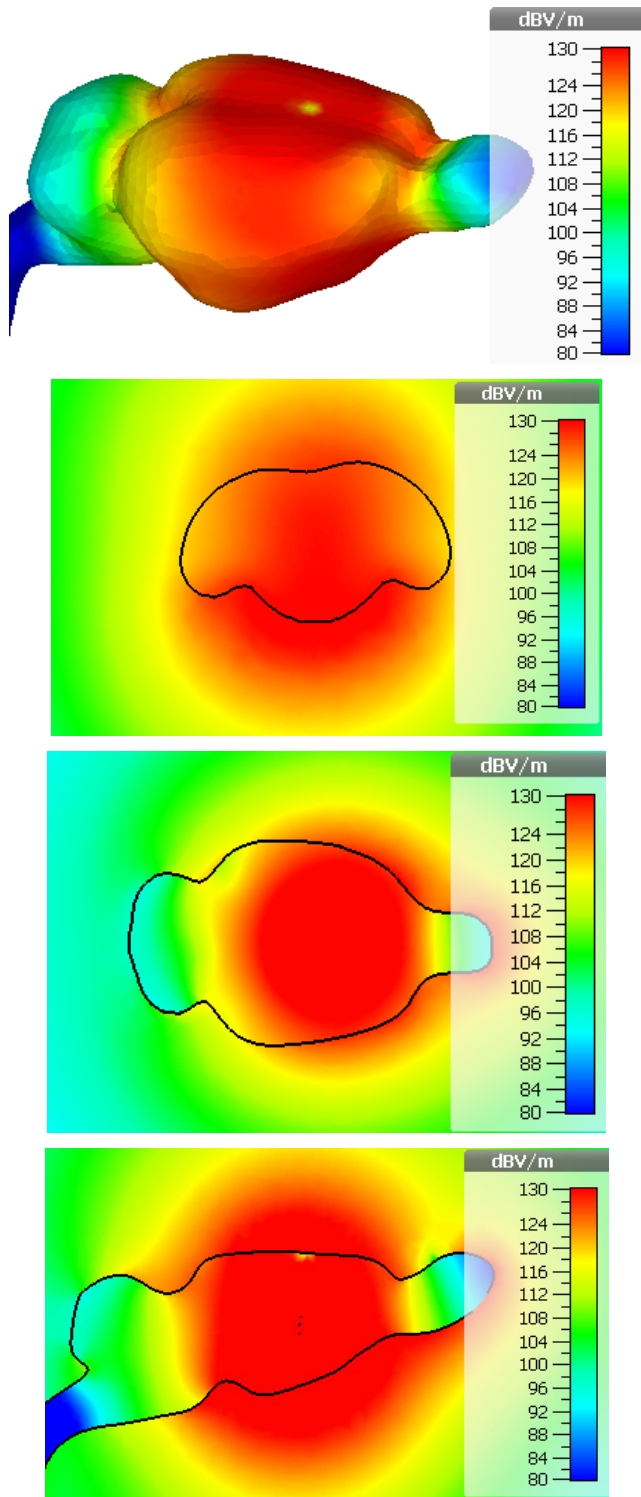


Fig. 8. Electric field distribution in model #1 evaluated by electro-quasi-static solver. From the top: the brain surface, the coronal cut, the axial cut and the sagittal cut.

The electro-quasi-static solver interacts with the brain model properly thanks to the long wavelength of the excitation signal and small electric dimensions of the model. Using the frequency scaling method [11] in conjunction with the full-wave time-domain solver, the frequency is shifted from 10 Hz to 10 MHz, the wavelength is shortened and electrical dimensions of the model are increased. Thus, the full-wave time-domain solver is not recommended to be used.

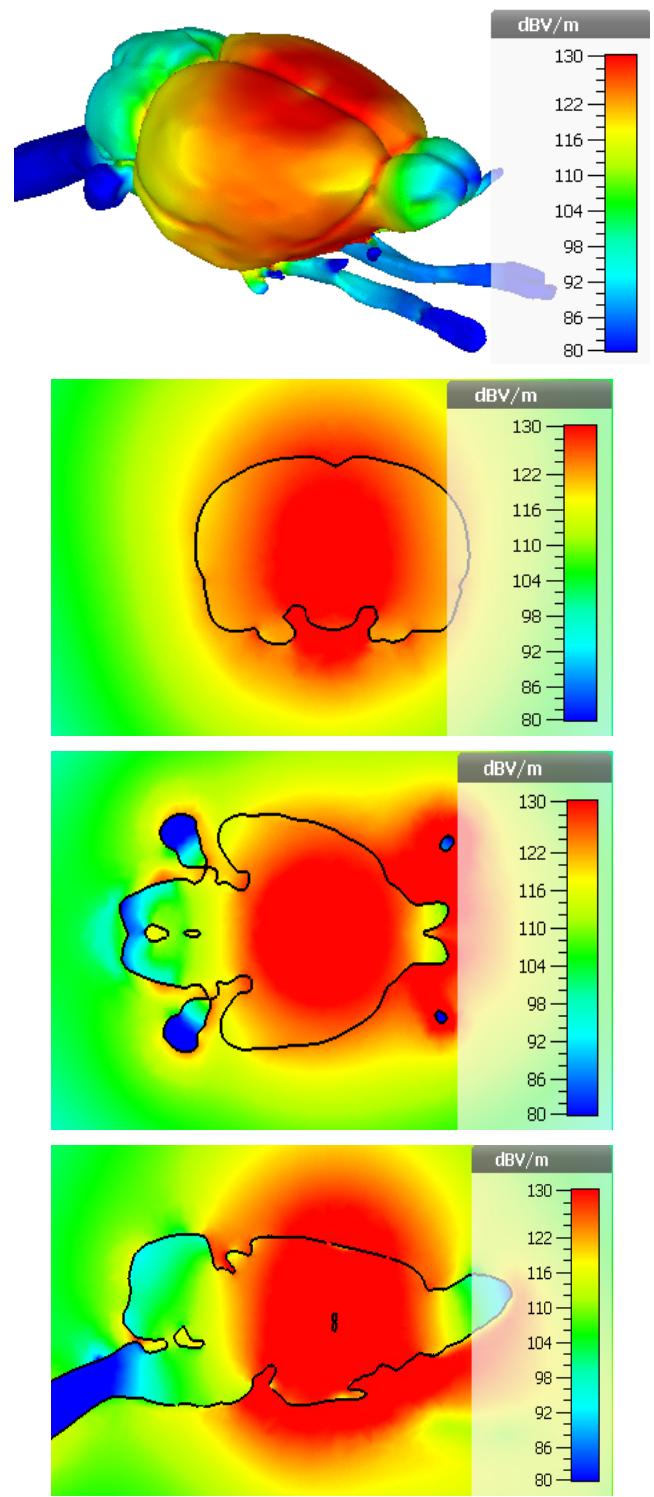


Fig. 9. Electric field distribution in model #2 evaluated by electro-quasi-static solver. From the top: the brain surface, the coronal cut, the axial cut and the sagittal cut.

3.3 Complete Head

The model #1 of rat's brain was converted to voxels, and completed by the cerebrospinal fluid and the skull. The measuring trajectory p_2 (the blue lines in Fig. 3) are measured from left to right (the horizontal axis in Fig. 10 and Fig. 11). Due to the stairway surface of voxel models, the

measuring trajectory was created on the top of models to follow the planar surface. That way, continuous dependencies without quick variations caused by sharp edges of voxels were obtained. Moreover, the measuring trajectory on the brain, the fluid and the skull can be of the same length.

In Fig. 10, the influence of the cerebrospinal fluid and the skull is shown. For the simulation of the brain model #1 completed by the fluid and the skull, the electro-quasi-static solver was used to compute electric field intensity along the trajectory p_2 . Comparison shows that the field distribution on the pure brain differs both in the magnitude and the shape. The attenuation of electric field intensity E is caused by transitions from the brain to the cerebrospinal fluid and from the fluid to the skull.

Electric field intensity on the pure brain reaches the maximum magnitude in the smallest distance from the excitation source. Increasing the distance from the source, the electric field intensity gradually attenuates. Nevertheless, the addition of the cerebrospinal fluid and the skull causes irregular distribution of electric field intensity E along the measuring trajectory p_2 .

The results show two parts of measuring trajectory p_2 where the electric field intensity E is higher for the complete model of the head. However, the results for the rest of the measuring trajectory p_2 indicate smaller values of electric field intensity E . Moreover, the electric field intensity E is attenuated faster when the distance increases from the maximum value compared with pure brain. Thus, the inclusion of more parts of rat's head enhances the accuracy of the forward modeling.

The complete head was simulated by the electro-quasi-static solver. The measuring trajectory p_2 was on the surface of separate models (see blue lines in Fig. 3). The position was the same for x, z coordinates and differed in y coordinate. A different y position corresponds to separate models (the brain, the cerebrospinal fluid, and the skull).

In Fig. 11, the distribution of electric field intensity E on surfaces of separate models is irregular due to the interface among models. Hence, the measuring position in rat's head is important for forward modeling and EEG measure-

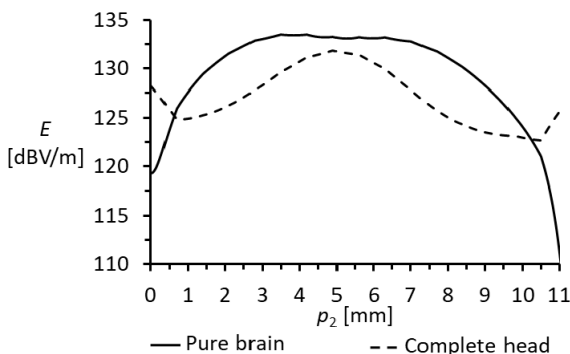


Fig. 10. Electric field intensity along the measuring trajectory p_2 : the influence of the cerebrospinal fluid and the skull.

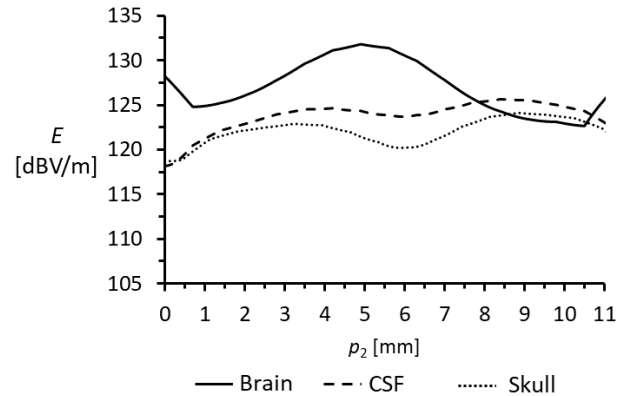


Fig. 11. Electric field intensity along the measuring trajectory p_2 : the brain (full line), the fluid (dashed line) and the skull (dotted line).

ment. In real EEG measurements, a small shift in the depth of measuring electrodes can give different results.

Figure 12 shows electric field distribution evaluated by the electro-quasi-static solver for the complete head on the surface of the brain, in the coronal cut, the axial cut and the sagittal cut passing the center of the head. In the picture of the field distribution on the brain (the top picture), the cerebrospinal fluid and the skull are hidden. The result indicates influence of separate head models to the distribution of electric field intensity.

4. Conclusions

In the paper, electromagnetic models of rat's brain and rat's head were described. Attention was turned to the discretization of the brain, the selection of the appropriate solver, and the composition of the whole head of the brain, the cerebrospinal fluid and the skull.

When applied to the spherical model of rat's head, comparison of CST solvers shows that the electro-quasi-static solver produces the minimum relative error compared to the analytical solution. On the other hand, the e-static solver shows the highest inaccuracy compared to the analytical solution. The frequency scaling method applied in the full-wave time domain method increases the relative error and produces results comparable to the stationary current solver. The full-wave frequency domain solver achieves the relative error comparable to the electro-quasi-static solver, but CPU-time demands are higher.

When changing the number of mesh elements, almost the same dependencies of electrical fields are obtained. The model defined by 94 084 tetrahedrons results in the same dependency as the model with the highest number of tetrahedrons. Nevertheless, the CPU-time demands are much higher for the model with the highest number of tetrahedrons. Thus, the smaller number of tetrahedrons is sufficient for forward modeling.

Since rat's brain cannot be approximated by a sphere, more realistic models of rat's brain were developed. The same electric-field dependencies were obtained when the

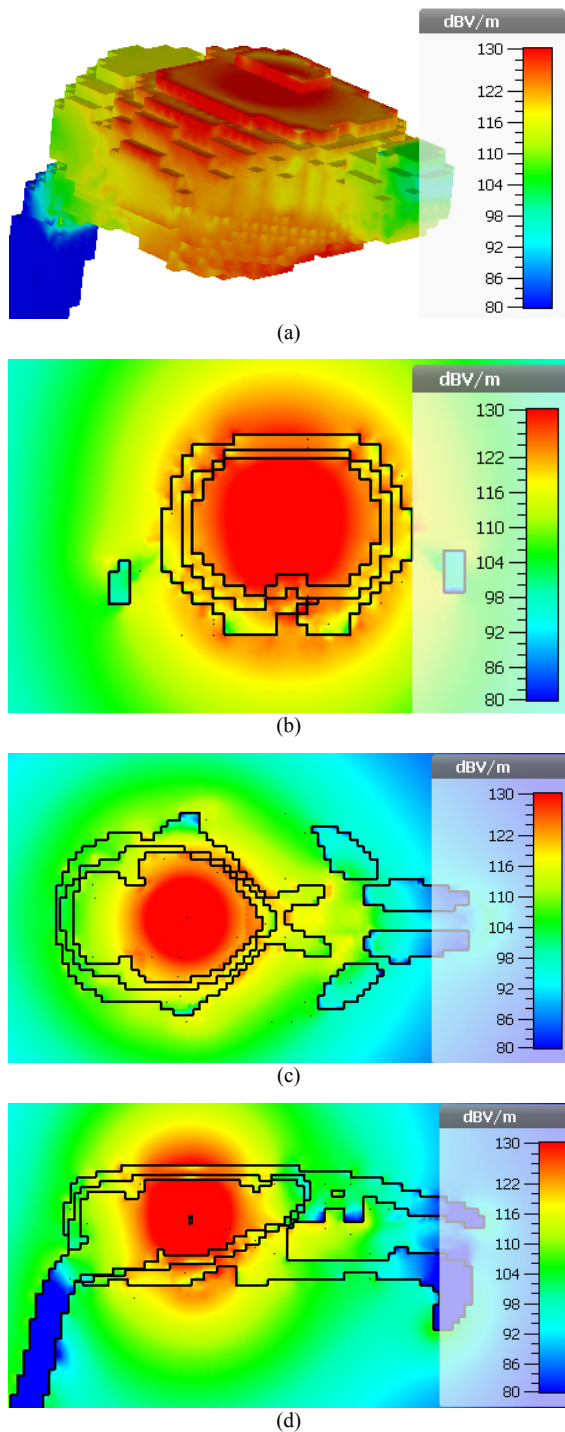


Fig. 12. Distribution of electric field intensity for complete rat's head model in the electro-quasi-static solver: (a) brain surface, (b) coronal cut, (c) axial cut, (d) sagittal cut.

e-static solver and the stationary current one were used. Nevertheless, the stationary current solver showed much smaller relative error compared to the e-static solver when the spherical brain was simulated. The stationary current solver is not suitable for realistic forward modeling.

Accuracy of the full-wave time-domain solver is related to the accuracy of the model geometry:

- In case of the fine model #2, the accuracy is comparable with the e-static solver and the stationary current one.
- In case of the rough model #1, the accuracy approaches the electro-quasi-static solver.

The error of the full-wave time-domain solver is caused by the frequency scaling method [11] which shifts the frequency of analysis from 10 Hz to 10 MHz. The higher frequency corresponds to the smaller wavelength, and the interaction of waves with the model is different.

The best results from the viewpoint of accuracy and CPU-time demands were reached by the electro-quasi-static solver which does not support simulations of lumped elements. Fortunately, simulations of lumped elements are supported by the full-wave frequency-domain solver with a similar relative error and higher CPU-time demands.

Comparison of all the solvers from the viewpoint of CPU-time demands showed that the e-static solver and the stationary current solver can save the CPU time compared to other solvers in case of the rough model #1. For the fine model #2, the CPU time demands were similar for all the solvers except of the full-wave time-domain one.

Comparison of all solvers shows that:

- The e-static solver and the stationary current one excel in CPU-time demands but fail in accuracy.
- The full-wave time-domain solver is not suitable for forward modeling if both the accuracy and CPU-time demands are considered at the same time.
- Both the electro-quasi-static solver and the full-wave frequency-domain solver excel in accuracy. When simulating simpler models, the full-wave frequency-domain solver requests more CPU time.

In order to create the model of the whole head, the rough brain model converted into voxels (the model #1) was completed by the cerebrospinal fluid and the skull. Thanks to the voxel conversion, the perfect alignment of the brain, the fluid and the skull was ensured, and the simulation was accelerated.

Comparison of the separate brain (converted to voxels) and the complete head indicates that dependencies for the separate brain differ in the magnitude and the shape. If the cerebrospinal fluid and the skull are added, the attenuation of the calculated signal can be observed. Moreover, the irregular distribution of electric field intensity was shown. If more parts of rat's head are included, a better accuracy of forward modeling is reached.

For the complete head, the irregular dependencies of the electric field intensity were obtained for the brain, the fluid and the skull surfaces. Therefore, the small change in depth can give a different value of electric field intensity. This irregular distribution is caused by interfaces of models with different permittivity and electric conductivity.

Spatial distributions of electric field intensity for the model #1, the model #2 and the complete model were visualized on the surfaces, and in the cut passing the center of the head (the coronal plane, the axial plane and the sagittal plane were considered). The result indicates the influence of separate parts of the head to the distribution of electric field intensity.

In near future, the numerical model of rat's head will be validated experimentally. Electrical potentials will be measured on the brain surface of a live rat in 13 different points. The numerical model of the brain will be calibrated to reach a reasonable agreement. The process of the calibration should indicate whether an isotropic model of the brain is sufficient for forward modeling, or anisotropy of the brain tissue is necessary to be considered.

Acknowledgment

The presented work was supported by the Czech Science Foundation under the grant no. 18-16218S. Simulations were performed in the SIX Research Center thanks to the support of the National Sustainability Program (the grant LO1401).

References

- [1] HE, B. *Neural Engineering*. 1st ed., rev. New York (USA): Kluwer Academic/Plenum, 2005. ISBN: 978-0-306-48609-8
- [2] KURATKO, D., RAIDA, Z., CUPAL, M., et al. Electromagnetic modelling of rat's brain: comparison of models and solvers. In *Proceedings of the International Workshop on Computing, Electromagnetics, and Machine Intelligence (CEMi 2018)*. Stellenbosch (South Africa), 2018, p. 31–32. DOI: 10.1109/cemi.2018.8610569
- [3] RAMIREZ, R. R. Source localization. *Scholarpedia*, vol. 3, no. 11. DOI: 10.4249/scholarpedia.1733 [Online] Cited 2018-11-12. Available at: http://www.scholarpedia.org/article/Source_localization
- [4] HALLEZ, H., VANRUMSTE, B., GRECH, R., et al. Review of solving the forward problem in EEG source analysis. *Journal of NeuroEngineering and Rehabilitation*, 2007, vol. 4, no. 1, p. 1–29. DOI: 10.1186/1743-0003-4-46
- [5] GOTO, T., HATANAKA, R., OGAWA, T., et al. An evaluation of the conductivity profile in the somatosensory barrel cortex of wistar rats. *Journal of Neurophysiology*, 2010, vol. 104, no. 6, p. 3388–3412. DOI: 10.1152/jn.00122.2010
- [6] BRETTE, R., DESTEXHE, A. *Handbook of Neural Activity Measurement*. 1st ed., rev. Cambridge (UK): Cambridge University Press, 2012. ISBN: 978-0-521-51622-8
- [7] POHL, B. M., GASCA, F., HOFMANN, U. G. *IGES and .STL File of Rat Brain*. [Online] Cited 2018-11-12. Available at: https://figshare.com/articles/IGES_and_stl_file_of_a_rat_brain/823546
- [8] PAPP, E. A., LEERGAARD, T. B., CALABRESE, E., et al. Waxholme space atlas of the Sprague Dawley rat brain. *NeuroImage*, 2014, vol. 97, p. 374–376. DOI: 10.1016/j.neuroimage.2014.04.001
- [9] KJONIGSEN, L. J., LILLEHAUG, S., BJAALIE, J. G., et al. Waxholm Space atlas of the rat brain hippocampal region: Three-dimensional delineations based on magnetic resonance and diffusion tensor imaging. *NeuroImage*, 2015, vol. 108, p. 441–449. DOI: 10.1016/j.neuroimage.2014.12.080.
- [10] SERGEJEVA, M., PAPP, E. A., BAKKER, R., et al. Anatomical landmarks for registration of experimental image data to volumetric rodent brain atlasing templates. *Journal of Neuroscience Methods*, 2015, vol. 240, p. 161–169. DOI: 10.1016/j.jneumeth.2014.11.005
- [11] JAIN, S., MITTRA, R., WIART, J. Full-wave modeling of brain waves as electromagnetic waves. *Progress in Electromagnetic Research*, 2015, vol. 151, p. 95–107. DOI: 10.2528/PIER15011404
- [12] –. *CST Studio Suite 2018* [Online] Cited 2018-11-12. Available at: <https://www.cst.com/>
- [13] NUNEZ, P. L., SRINIVASAN, R. *Electric Fields of the Brain: The Neurophysics of EEG*. 2nd ed. rev. New York (USA): Oxford University Press, 2006. ISBN 9780195050387
- [14] BUZSAKI, G. *Rhythms of the Brain*. 1st ed., rev. New York (USA): Oxford University Press, 2006. ISBN: 9780199828234
- [15] –. *Blender*. [Online] Cited 2018-11-12. Available at: <https://www.blender.org/>
- [16] –. *MeshLab*. [Online] Cited 2018-11-12. Available at: <http://www.meshlab.net/>
- [17] –. *Autodesk MeshMixer*. [Online] Cited 2018-11-12. Available at: <http://www.meshmixer.com/>
- [18] –. *Autodesk Fusion 360*. [Online] Cited 2018-11-12. Available at: <https://www.autodesk.com/products/fusion-360/overview>
- [19] SCHIMPF, P. H., RAMON, C., HAUEISEN, J. Dipole models for the EEG and MEG. *IEEE Engineering in Medicine and Biology Society*, 2002, vol. 49, no. 5, p. 409–418. DOI: 10.1109/10.995679
- [20] GUTIERREZ, Z., NEHORAI, A., MURAVCHIK, C. H. Estimating brain conductivities and dipole source signals with EEG arrays. *IEEE Transaction on Biomedical Engineering*, 2004, vol. 51, no. 12, p. 2113–2122. DOI: 10.1109/TBME.2004.836507
- [21] LAI, Y., VAN DRONGELEN, W., DING, L., et al. Estimation of in vivo human brain-to-skull conductivity ratio from simultaneous extra- and intra-cranial electrical potential recordings. *Clinical Neurophysiology*, 2005, vol. 116, no. 2, p. 456–465. DOI: 10.1016/j.clinph.2004.08.017
- [22] ANDREUCCETTI, D., FOSSI, R., PETRUCCI, C. *An Internet Resource for the Calculation of the Dielectric Properties of Body Tissues in the Frequency Range 10 Hz–100 GHz*. [Online] IFAC-CNR. Florence (Italy). 1997. Based on data published by C. Gabriel et al. in 1996. Available at: <http://niremf.ifac.cnr.it/tissprop/>

About the Authors ...

David KUŘÁTKO was born in 1993. He received his master degree at the Department of Radio Electronics, Faculty of Electrical Engineering and Communication, Brno University of Technology (FEEC BUT) in 2018 and his thesis dealt with modeling the brain of a rat, investigation of mathematical formulation of Maxwell equations which can be used for the development of forward models

and development of agar phantoms for experimental validation. He is currently a Ph.D. student at the Department of Radio Electronics FEEC BUT. His research interest is focused on forward modeling.

Daniel Krzysztof WÓJCIK received his M.Sc. and Ph.D. degrees at the Department of Physics of the University of Warsaw in 1996 and 2000, respectively. He was a research assistant at the Center for Theoretical Physics PAS 1996-2000. He worked at the Institute for Physical Science and Technology, University of Maryland (2000-2002) and School of Physics (2002-2003) on deterministic models of quantum walks which formed the basis of his habilitation (2008, Institute of Physics PAS). In 2003 he joined the Nencki Institute of Experimental Biology PAS where he is a professor and heads the Laboratory of Neuroinformatics.

Jaroslav LÁČÍK received the M.Sc. and Ph.D. degrees from Brno University of Technology, Brno, Czech Republic, in 2002 and 2007, respectively. He is currently an Associate Professor at the Department of Radio Electronics, Faculty of Electrical Engineering and Communication, Brno University of Technology. His research interests are antennas, body-centric wireless communication, and computational electromagnetics. He is a member of IEEE.

Vlastimil KOUDELKA was born in Usti nad Labem on April 1985. He received the M.Sc. and Ph.D. from Brno University of Technology, Brno, Czech Republic, in 2009 and 2014, respectively. He is currently a junior researcher at the National Institute of Mental Health in Klecany. Dr. Koudelka is involved in multimodal neuro-imaging techniques in human and EEG pre-clinical research in rats.